Microstructure fiber-based source of photonic entanglement

Journal:	*Journal of Selected Topics in Quantum Electronics*
Manuscript ID:	draft
Manuscript Type:	Invited
Date Submitted by the Author:	
Complete List of Authors:	Fan, Jingyun; National Institute of Standards and Technology, Optical Technology Division Migdall, Alan; National Institute of Standards and Technology, Optical Technology Division Chen, Jun; National Institute of Standards and Technology, Optical Technology Division Goldschmidt, Elizabeth; National Institute of Standards and Technology, Optical Technology Division Ling, Alexander; National Institute of Standards and Technology, Optical Technology Division
Keyword:	Optical Kerr effect

Microstructure fiber-based source of photonic entanglement

J. Fan, A. Migdall, J. Chen, E. A. Goldschmidt, and A. Ling

Abstract—**We review the development of photonic entanglement via four-wave mixing in microstructure fiber.**

Index Terms—**Microstructure fiber, four-wave mixing, correlation, entanglement.**

I. INTRODUCTION

ENTANGLEMENT, a quantum mechanical property with no classical counterpart, can help achieve great computing power and deliver information in a truly secure way. The past decade has witnessed rapid advancements in these directions. Entanglement with photonic qubits has unique advantages compared with other qubit candidates because photonic qubits are resistant to many decoherence mechanisms and are the fastest possible carriers of information. To date, entangled photons have been used for long-distance quantum-key-distribution [1][2], quantum logic operations [3-[5], and quantum teleportation of one- and two- qubit states [6]-[8]. The photons used for these applications have mainly been produced by optically pumping nonlinear media, utilizing either electronic transitions between energy levels or electron quivering in the external electric field. Such sources based on the material collective nonlinear response are inherently probabilistic, though modern experimental technology that allows for precise control of atomic transitions has led to the development of many potential on-demand photon sources

which are outside the scope of this review. The interactions in nonlinear media take place over finite spatial and temporal extensions, which can be equivalently represented by finite distributions in the energy and momentum domains. Theoretically, careful engineering of the temporal and spatial mode of the pump field and refractive-index matching between the pump and daughter fields can ensure that daughter photons are emitted in a single-spatial mode. However, such tasks can be technically challenging. Instead, for many quantum information processing experiments, a pinhole filter is simply placed in the emission field to approximate single-spatial mode output of daughter photons, leading to high losses of those photons. Daughter photons emitted into a single spatial mode can be collected with almost no loss, which is crucial for applications such as loop-hole free Bell test and quantum squeezing. Single mode optical fiber (SMF), which allows light waves to propagate only in a single transverse spatial mode, offers the potential for photons to be produced, collected, encoded, distributed and detected in a single-spatial mode. This has led to significant active research in the area of fiber-based quantum information processing. The quantum correlation between the daughter fields produced via four-wave mixing process in SMF was first reported in 2001 [9][10]. Since then, there has been significant progress in the development of fiber-based photonic entanglement. In this paper, we present a review of entangled photon sources based on a special class of SMF, called microstructure fiber (MF), which have been developed in recent years.

II. CREATION OF TWO-PHOTON LIGHT VIA FOUR-WAVE MIXING IN MICROSTRUCTURE FIBER

A. Spontaneous nonlinear optical process in optical fiber

SMF used in optical communications is made of glass material, which has inversion symmetry, causing the second-order nonlinear optical response to be absent. The potentially long interaction length in SMF allows otherwise weak third-order nonlinear optical effects to become noticeable. Various third-order nonlinear processes, such as four-wave mixing (FWM) and Raman scattering mutually stimulate each other. When the interaction strength is very weak (given by $PL \ll 1$, where P is the optical power and L is the optical pass length in SMF), these nonlinear processes are spontaneous and disentangled from each other. Only in this regime are we able

to examine the individual photon statistics of each nonlinear process separately. The FWM takes two photons from the pump field(s) (ω_p) to create a pair of signal (ω_s, $\omega_s > \omega_p$, $\Omega = \omega_s - \omega_p$, sometimes referred to as anti-Stokes photons) and idler (ω_i, $\omega_i < \omega_p$, $\Omega = \omega_p - \omega_i$, sometimes referred to as Stokes photons) photons that are bound by energy conservation, $\omega_s + \omega_i = 2\omega_p$. This is the principle on which MF sources of correlated photon pairs are based. In Raman scattering, pump photons couple to the thermal reservoir $[n(\Omega) = 1/(e^{\hbar\Omega/k_B T} - 1)]$ of SMF and scatter individually to either shorter or longer wavelengths. Photons produced via Raman scattering cover a more than 40 THz spectral range, and overlap the spectral range of the signal and idler photons from FWM. In practice, a signal photon and an idler photon are taken to be a correlated pair if they are detected at single-photon avalanche photodiode (APD) within a small time window, typically on the order of a few nanoseconds or less. Photons may be produced at the signal and idler wavelengths via Raman scattering within this time window. The induced accidental coincidences cannot be distinguished from the true two-photon coincidences from FWM. They appear as error bits, the frequency of which must be made small enough not to affect the integrity of information exchange.
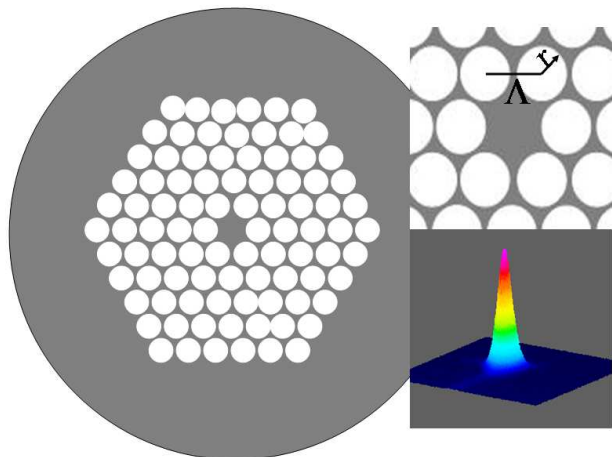

Fig. 1. A typical layout of microstructure fiber (MF) with a defect area surrounded by patterned air-holes. The zoom-in on the top-right shows the definitions of the air-hole size and the hole-to-hole separation, and the one on the bottom-right shows the single mode light output with $\lambda = 800$ nm from a MF.

The analysis of FWM, Raman scattering, and other nonlinear interactions in SMF has been delineated in the literature [11]. The descriptions given by both classical wave propagation theory and quantization method are consistent when the interaction strength is weak [12][13] and the scattering strength is linearly related to (PL) for Raman scattering and to $(PL/A_{eff})^2$ for FWM, where A_{eff} is the effective mode area in SMF. A higher pump power and a long SMF favor FWM at the cost of increased probability to emit multi-photon pairs [14]. The recent invention of the microstructure fiber provides an alternative solution.

B. Engineering the dispersion property of microstructure fiber

The guidance of light in a single transverse spatial mode in SMF is realized by matching a pair of parameters: the fiber core size and refractive index difference between the core glass and cladding glass [11]. In optical communications, a relatively large core diameter and a small refractive index difference are selected to optimize the confinement of the light field inside the fiber and minimize the optical nonlinear effect. MF, on the other hand, is designed to have a pattern of air holes run through the bulk fused silica material with one air hole missing (see Fig. 1). The refractive index of the defect area is $n = 1.45$ and the effective refractive index of the surrounding area can be close to 1 by having most of the region filled with air. With $\Delta n \approx 0.45$, the average diameter of the core size can be reduced significantly, for example, to $\approx 1\mu m$ or less, while still maintaining efficient single-mode confinement of light. The MF is called spectral-endless SMF because it can guide light with wavelengths ranging from 400 nm to 1700 nm in a single transverse spatial mode [15]. With the effective mode area reduced by 50 times, the interaction strength (PL) can be reduced by a factor of 50 while
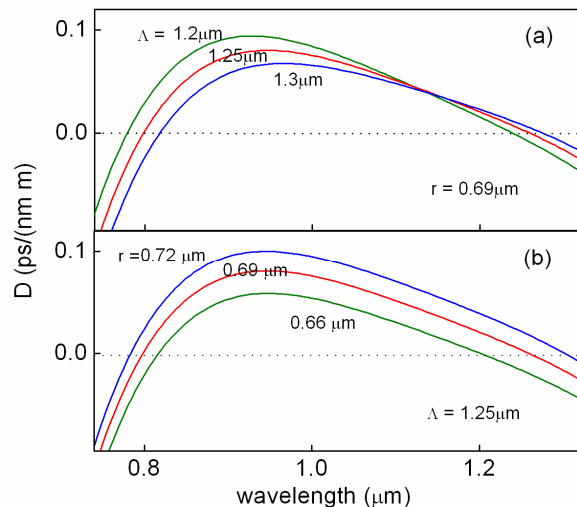
Fig. 2. Calculated dispersion of MF with different sets of air hole size and hole-to-hole separation. Note that the unit for dispersion is ps/nm/m.

maintaining similar FWM gain to that in standard SMF. This means that single photon noise, which is mainly due to Raman scattering, is suppressed by a similar amount.

TABLE I
FIBER ZERO-DISPERSION WAVELENGTH

r (μm)	Λ (μm)	λ_{ZDW1}(μm)	λ_{ZDW2}(μm)
0.69	1.20	0.778	1.249
	1.25	0.796	1.276
	1.3	0.813	1.294
Λ (μm)	r (μm)	λ_{ZDW1}(μm)	λ_{ZDW2}(μm)
1.25	0.66	0.812	1.198
	0.69	0.796	1.276
	0.72	0.782	1.354

Numerical studies show that the dispersion magnitude of

MF is bigger than that of conventional SMF by 10 times and the dispersion of MF is very sensitive to the variation of air hole size (r) and hole-to-hole separation (Λ) (see Fig. 2 and Table I).

Typical MF has two zero-dispersion-wavelengths (λ_{ZDW}), which are displaced by a significant amount for small variations of r or Λ. As shown in Fig. 2, both λ_{ZDW} are red-
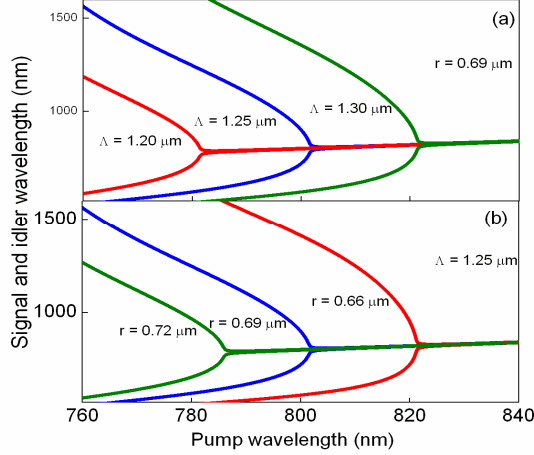

Fig. 3. Simulation of FWM in MF with the dispersion properties presented in Fig. 2. The four optical fields are assumed to be parallel-polarized and the pump fields are taken to be frequency-degenerate. The wavelengths of signal and idler photons at the peak gain of FWM are solved using the phase-matching equation, $\Delta k = (k_s + k_i - 2k_p) + 2\gamma P = 0$, where k_m with m = s, i, p are wave-numbers for the four interacting optical fields in FWM, and γP is 0.1 m^{-1}

shifted for increased Λ. For increased r, the short λ_{ZDW} is blue-shifted while the long λ_{ZDW} is red-shifted.

As an example, we numerically simulate the FWM phase-matching in MF with dispersion properties outlined in Fig. 2. The wavelengths of signal and idler photons created via perfectly phase-matched FWM (i.e., $\Delta k = (k_s + k_i - 2k_p) + 2\gamma P = 0$) are plotted as a function of the pump wavelength in Fig. 3, and exhibit significant dependence on r and Λ.

The flexibility in engineering the fiber dispersion is particularly important to the development of a MF-based photon-pair source. As discussed earlier, Raman scattering provides a noise floor to the photon pairs produced via FWM. The influence of Raman scattering can be characterized using a photon-counting method [16][17]. Using the single-channel detection rate of the signal and idler photons (D_{signal} and D_{idler}), the signal-idler coincidence rate (D_{coin}), the rate of accidental coincidences (D_{acci}), and the collection efficiencies for the signal and idler photons (η_{signal} and η_{idler}), the single photon and two-photon production rates in the MF can be estimated as

$$N_{pair} = \frac{D_{coin} - D_{acci}}{\eta_{signal}\eta_{idler}}, \qquad (1a)$$

$$N_{idler} = \frac{D_{idler} - D_{idler-background}}{\eta_{idler}} - N_{pair}. \qquad (1b)$$

The single photon production rate can be further linked to the Raman resonance as

$$N_{idler} = R(\Delta\omega)L_{eff}BP(1 + \frac{1}{e^{\hbar\Delta\omega/k_B T} - 1}), \qquad (2)$$

where $R(\Delta\omega)$ is the Raman gain spectrum, L_{eff} is the effective fiber length, B is the photon collection bandwidth, and the last term accounts for the phonon distribution. Thus the Raman gain spectrum can be measured. Experimental measurements of the Raman spectrum taken in this way are consistent with
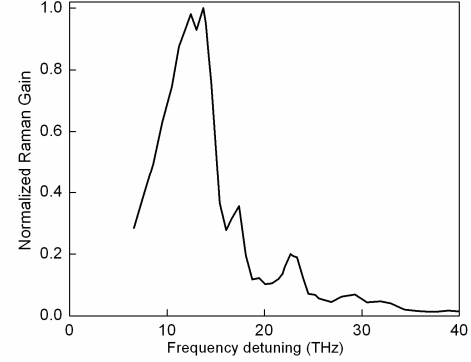

Fig. 4. Extracted Raman gain spectrum using the photon counting method in a fiber FWM process. $\lambda_{ZDW} \approx 745$ nm, $\lambda_p = 741.7$ nm, and $\gamma PL_{eff} = 0.1$.

the published result (see Fig. 4) [18].

The measured Raman gain spectrum provides a reference in engineering FWM in MF. As shown in Fig. 3, with appropriate dispersion engineering and choice of pump wavelength, the peak of FWM gain can be spectrally mapped out of the Raman resonance. This practice has been successfully used to produce high quality photon pairs. Additionally, with a large frequency detuning, pump photons can be better filtered out [17][19][20].

C. Creation of photon pairs via degenerate-pump four-wave mixing in MF

The process of FWM in an optical fiber involves four optical fields. The interaction Hamiltonian can be written as

$$H_{int} \sim \varepsilon_0 \chi^{(3)}_{ijkl}(\omega_1, \omega_2, \omega_3, \omega_4)$$
$$E_i(\omega_1)E_j(\omega_2)E_k(\omega_3)E_l(\omega_4) \qquad ,(3)$$

where $i, j, k, l = x, y$ account for the two transverse polarization directions and each optical field is decomposed into the positive and negative frequency parts, $E_i = E_i^{(+)} + E_i^{(-)}$. The interaction Hamiltonian allows the operation of FWM in a variety of modes. According to the nonlinear dielectric tensor, FWM can occur with four optical fields in parallel polarization [$\chi^{(3)}_{xxxx}$], with cross-polarized pump fields producing cross-polarized daughter fields [$\chi^{(3)}_{xyxy}$], or with parallel-polarized pump fields producing orthogonally polarized daughter fields [$\chi^{(3)}_{xxyy}$]. The relative interaction strengths of these processes are $\chi^{(3)}_{xyxy} = \chi^{(3)}_{xxyy} = \frac{1}{3}\chi^{(3)}_{xxxx}$, when all optical fields are parallel-polarized, the interaction strength is the strongest. The time reversal symmetry of the interaction Hamiltonian allows

FWM to occur in both forward and backward directions. The experiment presented below describes this operational mode
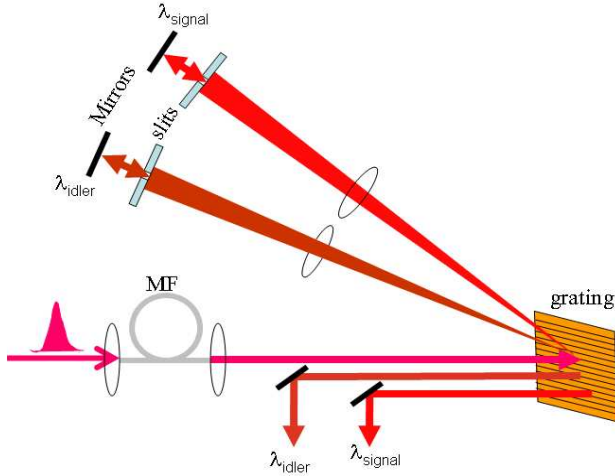

Fig. 5. Schematic for producing photon pairs in MF via FWM and the design of our double-pass spectrometer to spectrally select frequency-correlated signal and idler photon pairs from the broadband output of FWM.

and uses frequency-degenerate pump photons [21].

A linearly polarized laser pulse with duration of 8 picoseconds and $\lambda_p = 735.7$ nm is coupled into a 1.8 m MF with $\lambda_{ZDW} = 735 +/- 5$ nm at a repetition rate of 76 MHz. The polarization of the pump field is oriented along one of the fiber's principal axes. The output from the MF is directed to a home-made spectrometer, which consists of a reflection grating (1800 lines/mm), two $f = 750$ mm lens, two mirrors at the lens focus, and two translational and width-adjustable slits in front of the mirrors. Each lens-mirror pair re-images the photons at the selected wavelengths (λ_s and λ_i) back to the grating. After the second reflection on the grating, the selected photons are collected into SMFs and fed into single photon APDs (see Fig. 5). Such a spectrometer enables simultaneous selection of photons at multiple wavelengths and high efficiency spectral filtering. It also maintains optical alignment during wavelength selection, which proves to be very useful in finding frequency-correlated signal and idler photon pairs.

The recorded one- and two-photon count rates are plotted in Figs. 6(a) and 6(b), respectively, for an average pump power up to 1 mW. These numbers are used to calculate the production rates of single photons and photon pairs in the fiber according to Eq. (1). By translating the slits in the spectrometer, photon emission from the fiber nonlinear processes can be examined over a broad spectral range. With the extracted single-photon production rate, the Raman spectrum can be derived, and is plotted in Fig. 4.

A useful parameter to characterize the quality of photon pairs obtained from the fiber parametric process is to calculate the ratio of the measured coincidence rate to the accidental coincidence rate (C/A). With frequency detuned by ~30 THz from the pump, which puts the signal and idler photons outside the main Raman resonance, the photon-pair source has high purity. Very high C/A is measured at lower pump power [Fig. 6(c)]. Such a two-photon source can be converted into a heralded single photon source for information exchange, in which the detection of one photon heralds the presence of its frequency-correlated partner. A finite C/A corresponds to a bit-error-rate (BER) of $A/(C+A)$ for this type of operation. The two-photon source can also be converted into a polarization-entangled two-photon source using a second copy of the same source in which the produced photon pairs are orthogonally polarized (see Sec. III). The detection rate of two-photon entanglement will remain the same. The upper limit for the visibility of the two-photon polarization entanglement is $V = (C/A -1)/(C/A+1)$, and the introduced BER is given by $(1-V)/2 = A/(C+A)$, which is the same as the heralded single-photon scheme. Thus a high quality two-photon source is fundamentally important to developing a high quality entangled photon source. In the present measurement, the two-photon signal is detected at a rate of 38 kHz with $C/A = 10$, and an average pump power of 1 mW. The BER is 9%. Higher visibility and lower BER can be obtained by using lower pump powers with the trade-off of lower two-photon count rate (see
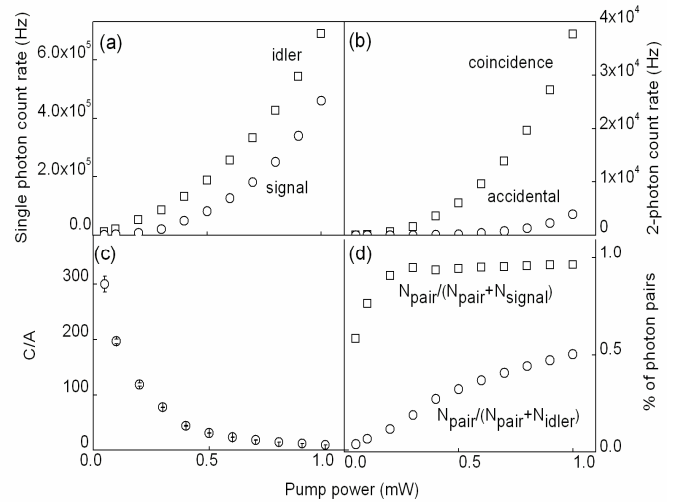

Fig. 6. (a) Single photon count rate at signal ($\lambda_s = 688.5$ nm) and idler (λ_i=790 nm) wavelengths as a function of pump power. $\Delta\lambda = 0.9$ nm. (b) Coincidence and accidental coincidence count rate as a function of pump power. (c) Ratio between the coincidence and accidental coincidence count rates. (d) Estimated percentage of produced 2-photons among all photons produced at the signal and idler wavelength, $\Delta\lambda = 0.9$ nm. The collection efficiencies are measured to be $\eta_s = 0.096$ for the signal photon and $\eta_i = 0.08$ for the idler photon. Fiber parameters: $\lambda_{ZDW} = 735$ nm, $\gamma = 100$ W^{-1}km^{-1}, fiber length = 2 m.

Figs. 6(b) and 6(c)).

Based on the estimated production rates of single photons and photon pairs in the fiber, we can see in Fig. 6(d) that with a large frequency detuning, FWM is the dominant nonlinear process at the signal wavelength even at low pump powers, while Raman scattering dominates at the idler wavelength for all studied powers. This is because the population of optical phonons decreases rapidly with increased energy, making the anti-Stokes Raman scattering (which falls into the signal wavelength band) less likely to occur in the fiber than its Stokes counterpart (which falls into the idler wavelength band).

D. Creation of frequency- degenerate photon pairs via reverse four-wave mixing in MF

In the last section, we discussed the use of frequency-degenerate pump fields to produce non-degenerate photon

pairs. However, many quantum information applications (for example, many interferometric-based quantum logical operations [22]), require frequency-degenerate photon pairs. The time reversal symmetry of the interaction Hamiltonian in Eq. (3) seems to suggest that the frequency-degenerate photon pairs can be produced by reversing the experiment described above. However, we explain below why this is not exactly the case.

In the experiment described above, the phase-mismatch for the forward FWM in the MF is given by $\Delta k_{\text{forward}} = (k_s + k_i - 2k_p) + 2\gamma P$. In a reversed configuration, the phase-mismatch for the backward FWM in MF is given by $\Delta k_{\text{backward}} = -(k_s + k_i - 2k_p) + \gamma(P_s + P_i)$. The Kerr nonlinearity, which contributes a self-phase modulation term, a scalar to the phase-matching condition, makes the forward and backward FWM processes different. When one FWM process occurs phase-constructively in the fiber, the other is less likely to build up.

The backward FWM can occur phase-constructively in the fiber with appropriate dispersion management. Several experiments have been reported that produce frequency-degenerate photon pairs using reversed non-degenerate-pump FWM process in fiber [23][24]. Here we describe the earliest
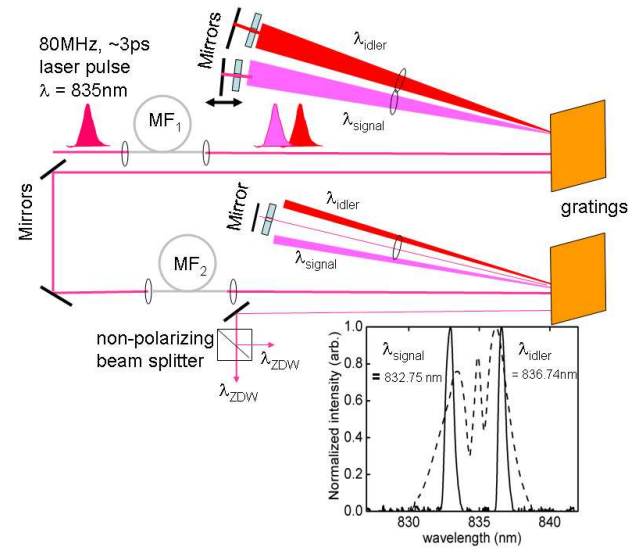

Fig. 7. Schematic for cascaded FWM using two identical pieces of MF to produce frequency-degenerate photon pairs. The inset shows that the dual pump wavelengths incident into the second MF are carved from the broadened spectrum of the laser pulse after propagation in the first MF.

one [23].

The dual pump wavelengths (λ_s, λ_i) are selected to be frequency-conjugate with respect to the fiber zero-dispersion wavelength λ_{ZDW} and also close to λ_{ZDW} such that phase-matching can be met or nearly met. In the experiment, we choose to use two pieces of identical MF. The dual wavelengths are carved from the broadened spectrum of the pump pulse after propagation in the first MF using a home-made spectrometer, the design of which is discussed above. The selected dual wavelengths are then coupled into the second MF. The output from the second MF is sent to a second home-made spectrometer. The selected photons at λ_{ZDW} are

sent to a 50/50 beam splitter. 50% of the photon pairs incident onto the beam splitter split into two single photons, which leave at different ports of the beam splitter and are coupled
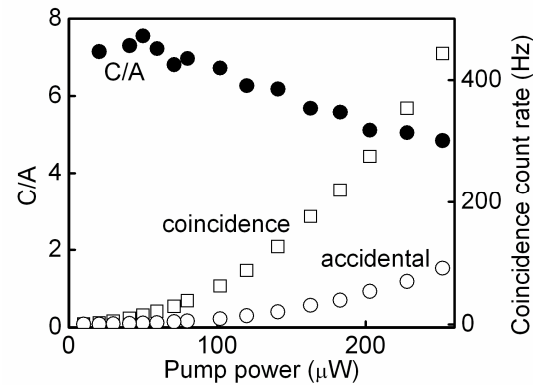

Fig. 8. Measurement of 2-photon coincidence in reverse FWM process. MF parameter: λ_{ZDW} = 835 nm, γ = 80 W^{-1}km^{-1}, fiber length = 2 m. Single photon collection efficiency η = 0.07, collection bandwidth $\Delta\lambda$ = 0.1 nm.

into single-photon APDs (see Fig. 7).

The detected photon-pair coincidence counts are plotted in Fig. 8, well above the noise floor given by the accidental coincidence counts. However, both the detected two-photon coincidence rate and the *C/A* are significantly lower than those measured in the degenerate-pump FWM experiments with a large frequency detuning (Fig. 6). This is because in this experiment, the wavelengths of the pump and daughter photons are very close to each other, and as a result Raman scattering is a larger effect. By decreasing the phonon population in the fiber with a thermal bath, for example cooling down the fiber to liquid nitrogen or liquid helium temperature, Raman scattering can be suppressed and the quality of photon pairs can be significantly improved [25][26]. The real coincidence count rate should be twice of what is shown in Fig. 8 considering the 50% loss due to the beam splitter in the experiment. This loss can be avoided by using a reverse Hong-Ou-Mandel interferometer (also known as a deterministic quantum splitter [27]) instead of a regular beam splitter, which also improves the purity and usability of the split photon-pair state [28][29].

III. MICROSTRUCTURE-BASED SOURCE OF 2-PHOTON ENTANGLEMENT

A. Fiber Sagnac interferometer

In the last section, we mentioned that polarization-entangled photon pairs can be produced by matching two identical sources of photon pairs. Since the conventional SMF is cylindrically symmetrical and can be made uniform over long length, the two photon-pair sources can be prepared by optically pumping two identical FWM processes along any two orthogonal axes in the fiber. The photon-pair emission from this dual FWM configuration can be written as

$$\psi \sim \sqrt{p(0)}\left|0_s 0_i\right\rangle$$
$$+\sqrt{p(1)}\left(\left|1_s 1_i\right\rangle_x \left|0_s 0_i\right\rangle_y + \left|0_s 0_i\right\rangle_x \left|1_s 1_i\right\rangle_y\right) \quad (4)$$
$$+\sqrt{p(2)}\left(\left|2_s 2_i\right\rangle_x \left|0_s 0_i\right\rangle_y + \left|0_s 0_i\right\rangle_x \left|2_s 2_i\right\rangle_y + \left|1_s 1_i\right\rangle_x \left|1_s 1_i\right\rangle_x\right)$$
$$+\ldots$$

where the lowest, non-vacuum order is given by $\left(\left|1_s 1_i\right\rangle_x \left|0_s 0_i\right\rangle_y + \left|0_s 0_i\right\rangle_x \left|1_s 1_i\right\rangle_y\right)$, in which x and y stand for
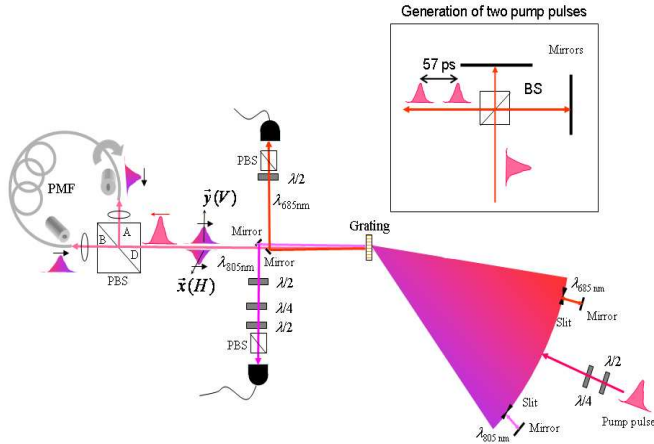

Fig. 9. Schematic for creation of polarization-entangled photon pairs using FWM in a Sagnac interferometer. PBS: polarizing beam splitter. BS: 50/50 non-polarizing beam splitter. $\lambda/2$ and $\lambda/4$ are half- and quarter wave plates. Inset is a Michelson interferometer to be inserted into the pump beam path to generate two identical pump pulses for the creation of time-bin entanglement.

orthogonal polarizations. This is commonly rewritten as $(H_s H_i + V_s V_i)/2^{1/2}$, where H and V each represent a single photon in horizontal or vertical polarization. The probability to emit multiple photon pairs can be efficiently suppressed by operating with smaller interaction strength.

To implement the dual FWM processes in MF, extra care must be taken. The inner physical structure of a MF is basically a web formed by thin silica membrane. The symmetry and uniformity of a MF are determined by the manufacture capability. In practice, it is difficult to produce a MF with both rotation symmetry with respect to the fiber optical axis and translational symmetry along the optical axis. In general it is impossible to find two highly nonlinear axes which have similar dispersion properties and remain orthogonal even for a short piece of MF.

The birefringence of a MF can be enhanced to make it a polarization-maintaining microstructure fiber (PMF), which has only one highly nonlinear axis. The dispersion properties can be very different for the slow and fast axes. Here we describe a Sagnac interferometer configuration using a short piece of PMF, with which we generated polarization-entangled photon pairs [30, 31].

In the proposed Sagnac interferometer (see Fig. 9), the principal axis of the PMF is oriented vertically at one fiber end and horizontally at the other fiber end, with each end facing a different port of a polarizing beam splitter (PBS). A linearly polarized light beam incident onto the PBS via one of the two unused ports will leave at the same port after propagation in the interferometer, with its polarization now rotated by 90º. A 45º oriented, linearly polarized laser pulse incident on the PBS

via one unused port will split into two identical pulses, with one H-polarized and the other V-polarized. The two pulses counter-propagate along the same highly nonlinear axis in the twisted PMF, driving two identical FWM processes. The photon pairs produced in the two FWM processes remain
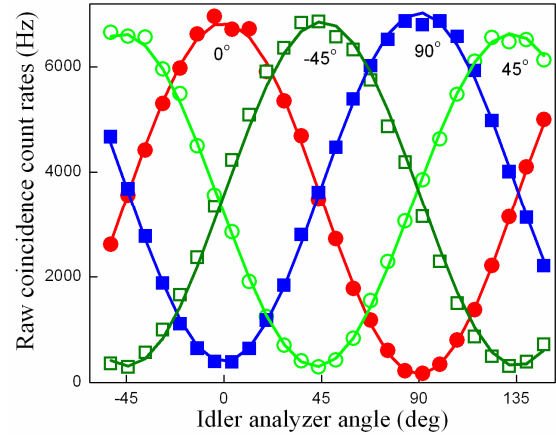

Fig. 10. Two-photon interference measurement on Bell state (HH-VV)/2$^{1/2}$ produced in a fiber Sagnac interferometer. PMF parameters: λ_{zdw} = 745 +/- 5 nm, nonlinearity γ = 70 W^{-1}km^{-1}, 2 meter. Pump parameters: λ_P = 740.7 nm, repetition rate: 76MHz., pump pulse duration: 10 ps. Collection parameter: λ_s = 689 nm and λ_i = 800 nm,, $\Delta\lambda$ = 0.9 nm. Photon collection efficiency: η_s = 0.08, η_i= 0.05.

linearly polarized and orthogonal to each other while counter-propagating in the PMF. They coherently interfere on the PBS, generating polarization-entangled photon pairs. It should be noted that these pairs are produced over the entire spectrum of FWM.

The frequency-matched signal and idler photon pairs are selected with a home-made spectrometer, in which the reflection grating is now replaced by a transmission grating to suit the current application. We studied the two-photon entanglement across a 20 nm spectral range. The detected two-photon coincidence rate remains at 7 kHz with the two-photon interference fringe visibility greater than 92% in the diagonal basis, with the corresponding BER = 4%. (A typical fringe measurement is shown in Fig. 10) [30].

The primary noise contribution is from Raman scattering. This is confirmed by studying the two-photon visibility at different interaction strengths. By decreasing the interaction strength to where the two-photon coincidence rate is 1 kHz, the visibility increases to greater than 98% for both the H/V and diagonal bases. Two-photon entanglement with such high visibility allows the source to be used in the test of both local and non-local hidden variable theories [32].

B. Hyper-entanglement

Entanglement in high dimensional Hilbert space is particularly useful to many quantum information applications [33][34]. It can be in the form of multi-party (photons, ions, or atoms) entanglement in a single degree of freedom (e.g., polarization), or a two-party system entangled in more than one degree of freedom. The latter is also known as hyper-entanglement [35]. Compared to multi-party entanglement, hyper-entanglement is more robust and easier to implement in practice. The two-photon polarization-entanglement discussed

in the previous section can be extended to a two-photon, four-qubit entanglement with a Michelson interferometer consisting of two mirrors and a 50/50 non-polarizing beam splitter.

The insertion of a Michelson interferometer into the pump beam path produces two identical pump pulses. The delay between them is set by the difference between the two beam paths in the Michelson interferometer. (See Fig. 9 inset). Coming out of the Michelson interferometer, the two pulses follow the same path of the original pump pulse to the Sagnac interferometer. Still working at the limit of weak interaction strength, the probability of emitting a photon pair via FWM is small, and the probability of producing a photon pair via FWM by either the first or the second pump pulse is equivalent. The
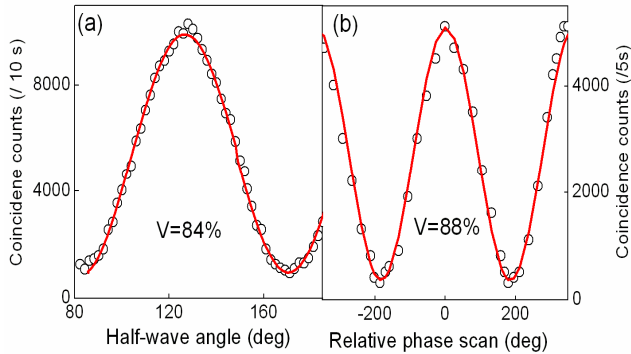

Fig. 11. Two-photon interference measurement on produced hyper-entangled Bell state $(|H_s\rangle|H_i\rangle + |V_s\rangle|V_i\rangle)\otimes(|0_s\rangle|0_i\rangle + |1_s\rangle|1_i\rangle)/2$ in the polarization space (a) and time-bin space (b). Parameters are the same as in Fig. 10.

wave function to describe the two-photon state is now written as $(|H_s\rangle|H_i\rangle + |V_s\rangle|V_i\rangle)\otimes(|0_s\rangle|0_i\rangle + |1_s\rangle|1_i\rangle)/2$, where $|0\rangle$ and $|1\rangle$ represents time bin 0 and time bin 1, corresponding to the creation of photon pair by either the first or the second pump pulse, respectively.

To examine the two-photon entanglement in both polarization and time-bin degrees of freedom, the two-photon interference is examined individually in the polarization space and time-bin space. The examination of time-bin entanglement is similar to the path-entanglement. By delaying the two-photon state in time bin $|0\rangle$ to coherently overlap with the two-photon state in time-bin $|1\rangle$, the two-photon interference visibility can be measured. The measured two-photon interferences are presented in Fig. 11, with visibilities greater than 84% for both polarization and time-bin entanglement [36]. The reason for the lower visibility (compared to the measurement in Fig. 10) is because of the spatial mode mismatch between $|H_s\rangle|H_i\rangle$ and $|V_s\rangle|V_i\rangle$ states and temporal mode mismatch between $|0_s\rangle|0_i\rangle$ and $|1_s\rangle|1_i\rangle$ states. Careful alignment brings the visibilities up to 99% as shown in later experimental studies [37].

In addition to the polarization and time-bin entanglement, path entanglement can be also implemented using a fiber-based two-photon source. Reviewing the design of the Sagnac interferometer in Fig, 9, polarization entanglement is produced after the polarizing beam splitter eliminates the polarization and path information carried by photon pairs from port A and port B. Simply replacing the polarizing beam splitter with a non-polarizing beam splitter and keeping the fiber principal

axis oriented in the same direction at both fiber ends, one can produce photon pairs described by $(|A_s\rangle|A_i\rangle + |B_s\rangle|B_i\rangle)/2^{1/2}$, representing a path-entangled two-photon state.

IV. FUTURE WORK

The development of a microstructure fiber-based source of photonic entanglement has made great progress in the past few years. The performance of such a source, measured by the two-photon spectral brightness and entanglement fidelity, is now approaching that of the best spontaneous parametric down conversion sources. The flexibility in engineering the fiber gain, dispersion, and birefringence, makes it possible to produce photonic entanglement over a wide spectral range, from the near ultraviolet to the infrared, to meet a broad range of applications.

While current microstructure fiber-based sources of photonic entanglement have many positive features, there are issues that need addressing to further improve these sources. For example, the quality of photonic entanglement can be sensitive to environmental or mechanical perturbations. The small fiber core size (≈ 1 μm) requires a high numerical aperture collection to couple light into and out of the fiber. Because of this, small mechanical drifts of the fiber tip can easily degrade two-photon visibility and collection efficiency, affecting the particular application at hand. Such instabilities can be greatly reduced by expanding the fiber core at fiber end to a more manageable size. Another issue that needs attention is the single photon collection efficiency. This efficiency can be quite low because the spectral filtering which is often necessary to generate high-purity photon pairs can be inefficient. Recent studies show that the signal and idler photon pairs produced via FWM in microstructure fiber can be spectrally factorable by judicious choice of fiber dispersion and pump wavelength [38], thus the spectral filtering requirement can be avoided. For a high flux of high fidelity entangled photon pairs, it is also necessary to operate at a high repetition rate while maintaining a low mean photon number per mode. This suppresses contamination from Raman scattering and multi-photon processes. In conclusion, the recent developments and research presented above demonstrate the great promise and challenges ahead for fiber-based sources of entangled photon pairs.

REFERENCES

[1] N. Gisin and R. Thew, "Quantum communication," *Nature Photonics* vol.1, pp. 165-171, Mar. 2007.

[2] R. Ursin, F. Tiefenbacher, T. Schmitt-Manderbach, H. Weier, T. Scheidl, M. Lindenthal, B. Blauensteiner, T. Jennewein, J. Perdigues, P. Trojeck, B. Omer, M. Furst, M. Meyenburg, J. Rarity, Z. Sodnik, C. Barbieri, H. Weinfurter, and A. Zeilinger, "Entanglement-based quantum communication over 144km," *Nature Physics*, vol. 3, pp. 481-486, July 2007.

[3] P. Walther, K. J. Resch, T. Rudolph, E. Schenck, H. Weinfurter, V. Vedral, M. Aspelmeyer, and A. Zeilinger, "Experimental one-way quantum computing," *Nature*, vol.434, pp. 169-176, March 2005.

[4] Kai Chen, Che-Ming Li, Qiang Zhang, Yu-Ao Chen, Alexander Goebel, Shuai Chen, Alois Mair, and Jian-Wei Pan, "Experimental realization of

one-way quantum computing with two-photon four-qubit cluster states," *Phys. Rev. Lett.* , vol. 99, pp. 120503-120507, Sept. 2007.

[5] Chao-Yang Lu, Xiao-Qi Zhou, Otfried Gühne, Wei-Bo Gao, Jin Zhang, Zhen-Sheng Yuan, Alexander Goebel, Tao Yang and Jian-Wei Pan, "Experimental entanglement of six photons in graph states," *Nature Physics*, vol. 3, pp. 91-95, Jan. 2007.

[6] D. Bouwmeester, Jian-Wei Pan, K. Mattle, M. Eibl, H. Weinfurter, and A. Zeilinger," Experimental quantum teleportation," *Nature*, vol. 390, pp. 575-579 Dec. 1997.

[7] Zhi Zhao, Yu-Ao Chen, An-Ning Zhang, Tao Yang, Hans J. Briegel & Jian-Wei Pan, "Experimental demonstration of five-photon entanglement and open-destination teleportation," *Nature*, vol.430, pp. 54-58, July 2004.

[8] Qiang Zhang, Alexander Goebel, Claudia Wagenknecht, Yu-Ao Chen, Bo Zhao, Tao Yang, Alois Mair, , Jörg Schmiedmayer , and Jian-Wei Pan, "Experimental quantum teleportation of a two-qubit composite system," *Nature Physics*, vol.2, pp. 678-682, Oct. 2006.

[9] Jay E. Sharping, M. Fiorentino, A. Coker, P. Kumar, and R. S. Windeler, "Four-wave mixing in microstructure fiber," *Optics Lett.*, vol. 26, pp. 1048-1050, July 2001.

[10] L. J. Wang, C. K. Hong, and S. R. Friberg, "Generation of correlated photons via four-wave mixing in optical fibres," *J. Opt. B: Quantum Semiclass Opt.* , vol. 3, pp. 346-352, Oct. 2001.

[11] G. P. Agrawal, *Nonlinear Fiber Optics*, New York, 1995.

[12] Paul L Voss and P. Kumar, "Raman-effect induced noise limits on $\chi^{(3)}$ parametric amplifiers and wavelength converters,", *J. Opt. B: Quantum Semiclass. Opt.*, vol. **6,** pp. 762-770, Aug. 2004.

[13] Q. Lin, F. Yaman, and Govind P. Agrawal, "Photon-pair generation in optical fibers through four-wave mixing: Role of Raman scattering and pump polarization," *Phys. Rev. A*, vol. **75**, pp. 023803-023822, Feb. 2007.

[14] E. A. Goldschmidt, M. D. Eisaman, J. Fan, S. V. Polyakov, and A. Migdall, "Spectrally bright and broad fiber-based heralded single-photon source," *Phys. Rev. A* vol. **78**, p. 013844, July 2008.

[15] P. S. Russel, "Photonic-crystal Fibers," *J. Lightwave Technol.*, vol.**24**, pp. 4729-4749, Dec. 2006.

[16] X. Li, P. L. Voss, J. Chen, K. F. Lee, and P. Kumar, "Measurement of co- and cross-polarized Raman Spectra in silica fiber for small detunings," *Opt. Express,* vol. **13**, pp. 2236-2244, March 2005.

[17] J. Fan and A. Migdall, "A broadband high spectral brightness fiber-based two-photon source," *Opt. Express,* vol. **15**, pp. 2915-2920, March 2007.

[18] R. H. Stolen and M. A. Bösch, "Low-frequency and low-temperature Raman-scattering in silica fibers," *Phys. Rev. Lett.*, vol.**48**, pp. 805-808, March 1982.

[19] J. G. Rarity, J. Fulconis, J. Duligall, W. J. Wadsworth, and P. S. Russel, "Photonic crystal fiber source of correlated photon pairs," *Opt. Express*, vol. **13**, pp. 534-544, Jan. 2005.

[20] J. Fulconis, O. Alibart, W. J. Wadsworth, P. S. Russel, and J. G. Rarity, "High brightness single mode source of correlated photon pairs using a photonic crystal fiber," *Opt. Express*, vol. **13**, pp.7572-7582, Sep. 2005.

[21] J. Fan, A. Migdall, and L. J. Wang, "Efficient generation of correlated photon pairs in a microstructure fiber," *Opt. Lett.*, vol. **30**, pp. 3368-3370, Dec. 2005.

[22] P.Kok, W. J. Munro, K. Nemoto, T. C. Ralph, J. P. Dowling, and G. J. Milburn, "Linear optical quantum computing with photonic qubits," *Rev. Mod. Phys.*, vol. **79**, pp. 135-174, Jan. 2007.

[23] J. Fan, A. Dogariu, and L. J. Wang, "Generation of correlated photon pairs in a microstructure fiber," *Opt.Lett.*, vol. **30**, pp. 1530–1532, Jun. 2005.

[24] J. Chen, K. F. Lee, C. Liang, and P. Kumar, "Fiber-based telecom-band degenerate-frequency source of entangled photon pairs," *Opt. Lett.*, vol. **31**, pp. 2798-2801, Sep. 2006. .

[25] H. Takesue and K. Inoue, "1.5-μm band quantum-correlated photon pair generation in dispersion-shifted fiber: suppression of noise photons by cooling fiber," *Opt. Express,* vol. 13, pp. 7832–7839, Oct. 2005.

[26] K. F. Lee, J. Chen, C. Liang, X. Li, P. L. Voss, and P. Kumar, "Generation of high-purity telecom-band entangled photon pairs in dispersion-shifted fiber," *Opt. Lett.*., vol. **31**, pp. 1905-1907, Jun. 2006.

[27] J. Chen, K. F. Lee, and P. Kumar, "Deterministic quantum splitter based on time-reversed Hong-Ou-Mandel interference," *Phys. Rev. A,* vol. **76**, pp. 031804(R), Sep. 2007.

[28] J. Chen, J. B. Altepeter, M. Medic, K. F. Lee, B. Gokden, R. H. Hadfield, S. W. Nam, and P. Kumar, "Demonstration of a quantum controlled-NOT gate in the telecom band," *Phys. Rev. Lett.*, vol. **100**, pp. 133603, Apr. 2008.

[29] J. Chen, J. B. Altepeter, and P. Kumar, "Quantum state engineering using nonlinear optical fiber Sagnac loop," *New J. Phys.*, vol. **10**, pp. 123019, Dec. 2008.

[30] J. Fan, M. D. Eisaman, and A. Migdall, "Bright phase-stable broadband fiber-based source of polarization-entangled photon pairs," *Phys. Rev. A*, vol. **76**, pp. 043836, Oct. 2007.

[31] J. Fulconis, O. Alibart, J. L. O'Brien, W. J. Wadsworth, and J. G. Rarity, "Nonclassical interference and entanglement generation using a photonic crystal fiber pair photon source," *Phys. Rev. Lett.*, vol. **99**, pp. 120501, Sept. 2007.

[32] M. D. Eisaman, E. A. Goldschmidt, J. Chen, J. Fan, and A. Migdall, "Experimental test of nonlocal realism using a fiber-based source of polarization-entangled photon pairs," *Phys. Rev. A*, vol. **77**, pp. 032339, March 2008.

[33] P. G. Kwiat and H. Weinfurter, "Embedded Bell-state analysis," *Phys. Rev. A*, vol. **58**, pp. R2623-R2626, Oct. 1998.

[34] C. Simon and J.-W. Pan, "Polarization entanglement purification using spatial entanglement," *Phys. Rev. Lett.*, vol. **89**, pp. 257901, Dec. 2002.

[35] P. G. Kwiat, "Hyper-entangled states," *J. Mod. Opt.*, vol. **44**, pp. 2173-2184, Nov. 1997.

[36] J. Chen, J. Fan, M. D. Eisaman, and A. Migdall, "Generation of high-flux hyperentangled photon pairs using a microstructure-fiber Sagnac interferometer," *Phys. Rev. A*, vol. **77**, pp. 053812, May 2008.

[37] E. A. Goldschmidt, M. D. Eisaman, J. Fan, S. V. Polyakov, J. Chen, and A. Migdall, "Spectrally Bright and Broad Fiber-Based Heralded Single-Photon Source," in *International Conference on Quantum Information*, (Optical Society of America, 2008), paper QWC4.

[38] K. Garay-Palmett, H. J. McGuinness, Offir Cohen, J. S. Lundeen, R. Rangel-Rojo, A. B. U'Ren, M. G. Raymer, C. J. Mckinstrie, S. Radic, and I. A. Walmsley, "Photon pair-state preparation with tailored spectral properties by spontaneous four-wave mixing in photonic fiber," *Opt. Express*, vol. 15, pp. 14870-14886, Oct. 2007.

Jingyun Fan received the B.S. degree in physics from University of Science and Technology of China and the PhD degree in physics from University of Maryland. He is a research faculty member of Joint Quantum Institute of University of Maryland and a guest researcher in National Institute of Standards and Technology. His current interest is on quantum and nonlinear optics, and laser-atom interaction.

Alan Migdall received the Ph.D. degree in physics from the Massachusetts Institute of Technology (MIT) and the B.S. degree in mathematics and physics from the University of Maryland. He is involved in projects that use two-photon light sources and their entanglement for absolute metrology and quantum information applications at the National Institute of Standards and Technology (NIST), Gaithersburg, MD, where he is also working on advancing single-photon technology for these applications. His previous work included the laser cooling of atoms, which resulted in the first trapping of a neutral atom. He has also organized a number of workshops, symposiums, and special issues on the topic as a means of encouraging single-photon technology. Dr. Migdall is a member of the Optical Technology Division at NIST, Gaithersburg and a fellow of the Joint Quantum Institute at the University of Maryland, College Park.

Jun Chen received the B.Sc. degree in physics from Peking University, Beijing, China in 1999, the M.Sc. degree in physics from Northwestern University, Evanston, IL in 2001, and the Ph.D. degree in Electrical Engineering and Computer Science from Northwestern University in 2007. From 2001 to 2007, he has participated in the experimental efforts of developing a fiber-based polarization entanglement source, both with non-degenerate photons and degenerate photons. Applications of such a source, such as long-distance quantum communication in optical fiber, a deterministic quantum splitter, and a quantum controlled-NOT gate, have been demonstrated. Since 2007, he has been a guest researcher at National

Institute of Standards and Technology, Gaithersburg, MD, and also affiliated with Joint Quantum Institute, University of Maryland, College Park. He has recently demonstrated hyper-entangled photon pairs from a photonic crystal fiber source, and highly pure, spectrally bright correlated photons from a chip-scale waveguide. His current research interests are quantum information processing in standard and novel optical fibers and waveguides, and classical nonlinear optics in those materials.

Elizabeth Goldschmidt is a Ph.D student at the Joint Quantum Institute at the University of Maryland, College Park and previously received a B.A. in physics from Harvard University. She is involved in research to develop single-photon and two-photon light sources as well as quantum memory systems for quantum information applications at the National Institute of Standards and Technology, Gaithersburg, MD.

Alexander Ling received his PhD from the National University of Singapore in 2008. He is currently working for the Joint Quantum Institute in Maryland, USA. His research interests are in the field of quantum optics; especially the generation and measurement of entangled light sources.